International Journal of Microwave and Wireless Technologies, 2017, 9(2), 437–446.
doi:10.1017/S1759078715001683

RESEARCH PAPER

Arc-cornered microstrip antenna with defected ground structure for broad banding and improved cross-polarization suppression over whole skew planes

SUBHRADEEP CHAKRABORTY AND SUDIPTA CHATTOPADHYAY

Defected ground structure (DGS)-integrated arc-cornered rectangular microstrip antenna (RMA) has been investigated to achieve broadband along with high co-polarized to cross-polarized radiation (CP–XP) isolation over principal as well as over skew planes without affecting the dominant mode co-polarized (CP) radiation pattern. The present arc-cornered RMA on circular and rectangular dot-type DGS is thoroughly studied and compared with the conventional rectangular microstrip antenna. In the present paper, a crucial emphasis is given to improve CP–XP isolation in all the skew planes and by employing circular dot-type DGS around 20 dB CP–XP isolation is achieved over whole skew planes as well as in the H-plane with the proposed structure with 20% impedance bandwidth. On the contrary, the CP–XP isolation and impedance bandwidth vary in opposite manner in case of the rectangular dot-type DGS. Around 25 and 10 dB CP–XP isolation with 9 and 22% impedance bandwidth have been obtained with thin and thick rectangular dot-type DGS, respectively. The corners of the patch surface are rounded in such a way to reduce spurious radiations from the sharp corners, which are generally attributed for high XP radiation along the diagonal directions.

Keywords: Antenna design, Modeling and measurements, Antennas and propagation for wireless systems

Received 13 June 2015; Revised 3 November 2015; Accepted 5 November 2015; first published online 7 December 2015

I. INTRODUCTION

Conventional rectangular microstrip antenna (RMA) is the most useful low-profile radiator due to its number of advantages such as, light weight, small size, low-cost, etc. [1, 2]. Hence, it finds the increasing number of applications day by day. However, these radiators have two main drawbacks. First of all, it is inherently a narrow band structure (around 5%). Secondly, it radiates significant amount of cross-polarized (XP) radiation with its normal linearly polarized broadside co-polarized (CP) radiation. Hence, it degrades the polarization purity (CP–XP isolation) of such radiators [2]. This XP radiation becomes more significant in the *H*-plane than in the *E*-plane [3] if the comparison is made between principal planes. However, the XP radiation from RMA is comparatively a bit low in the principal *H*-plane with its peak values in other skew planes and especially in the 45° diagonal plane [4, 5]. This puts evidently a restriction to its applications, such as in adaptive antenna arrays for cellular, mobile land, or other wireless communications, where wide coverage is usually required as indicated in [6]. Therefore, the enhancement of bandwidth along with improvement in polarization purity is the key issue of the research in the field of microstrip antennas.

Several investigations [7–9] were reported by modifying the feed structure and shape of the patch for broadening the bandwidth of such antennas. L-probe fed inverted EE-H-shaped slotted RMA has been employed in [7] for high-gain, broad bandwidth. However, this structure is very complex and suffers from poor polarization purity (only 12 dB CP–XP isolation) in its *H*-plane. Around 30% impedance bandwidth along with only 7 dB CP–XP isolation with E-shaped patch has been reported in [8]. Another report [9] shows that around 54% impedance band width can be achieved with Ψ-shaped patch. However, the presented patch in [9] shows very poor polarization purity at high frequencies where XP is comparable with CP radiation.

The employment of defected ground structure (DGS) to improve XP radiation for RMA is reported in [10–12]. These reports show the use of elliptical [10], linear bracketed [11], and simple slot-type [12] DGS in RMA where 15–25 dB of XP suppression compared with conventional RMA is revealed with poor impedance bandwidth. Around 6% impedance bandwidth can be obtained from [10, 12], while it is claimed in [11] that the wide impedance bandwidth (around 11%) can be obtained by employing bracketed DGS with RMA. The concept of defected patch surface to improve XP

Department of Electronics and Communication Engineering, Siliguri Institute of Technology, P.O. Sukna, Darjeeling, Siliguri 734009, West Bengal, India. Phone: 08967885437
Corresponding author:
S. Chakraborty
Email: deepc.jpg@gmail.com

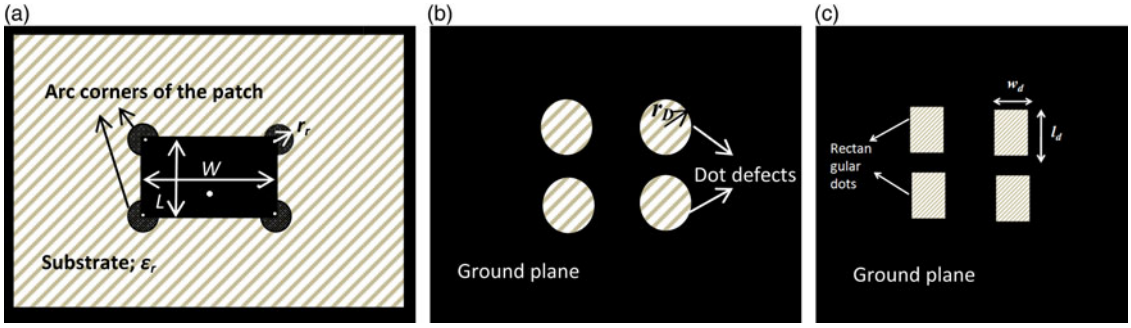

Fig. 1. Schematic representation of present DGS-integrated arc-cornered RMA on the 80 × 80 mm² ground plane: (a) top view, (b) bottom view with circular dot-type DGS, and (c) bottom view with rectangular dot-type DGS.

performance and bandwidth [13, 14] by the present authors is relatively a new technique, where arc and dumbbell-shaped defects have been employed on the surface of patch with circular and rectangular geometries, respectively. Around 16% impedance band width with more than 25 dB of CP–XP isolation is revealed in [14] for RMA. One very recent report [15] shows the theoretical analysis of rectangular-headed dumbbell DGS-integrated RMA, where around 25 dB of CP–XP isolation is achieved for all width to length ratios (0.8 to 1.6) of a patch.

However, the most critical point is that earlier no literatures are found except [11, 14], where the XP performance of RMA has been investigated in the planes other than principal planes, i.e. in diagonal skew planes. The suppression of XP fields in principal planes does not effectively suppress the XP radiation in diagonal or other skew planes. This in fact produces severe restrictions to the scientific community looking for such antennas with completely good polarization purity in all principal and other diagonal skew planes. The completely pure polarization in all principal and other skew planes is very much required for several wireless communication systems and especially for array applications and polarization reuse purpose. In the above-mentioned literatures [11, 14], the XP performances in the diagonal skew planes have been predicted with simulation results only and those are not supported by the measured data. Around 22 dB of CP–XP isolation in the principal *H*-plane is apparent from [11], while it produces only 12 dB of CP–XP isolation in the 45° diagonal planes. Similarly, more than 25 dB of CP–XP isolation in the principal *H*-plane is evident from [14] with only 16 dB of CP–XP isolation in the 45° diagonal planes. The conventional RMA with circular headed dumbbell DGS has been investigated by the present authors [16] recently which shows around 19 and 16 dB of CP–XP isolation in the principal *H*- and 45° diagonal planes, respectively. Moreover, around 22% band width along with 9.5 dBi gain is apparent from the reported structure [16]. Nevertheless, the CP–XP isolation is not uniform in the principal *H*- and 45° diagonal planes. Moreover, the CP–XP isolation in other diagonal skew planes has not been investigated in the work. Therefore, more thorough investigations are required to obtain complete polarization purity in all skew planes and it is a major challenge to the researchers working in the field of wireless communication.

To remove the shortcoming of earlier investigations and to take care of impedance bandwidth and XP performance simultaneously, a simple arc-cornered RMA with circular and rectangular dot-type defect in the ground plane has been investigated respectively as shown in Fig. 1. The circular dot-type DGS-integrated arc-cornered RMA can improve the bandwidth and at the same time produces improved CP–XP isolations in principal and all other diagonal skew planes. Around 19–20 dB of CP–XP isolation in all the planes (principal and diagonal skew planes) along with 20% impedance band width is revealed from the circular dot-type DGS-integrated arc-cornered microstrip antenna. On the contrary, the rectangular dot-type DGS-integrated arc-cornered RMA with thin defect width w_d offers excellent CP–XP isolation of 25 dB with poor (9%) impedance bandwidth. The present investigation demonstrates that this impedance bandwidth of the rectangular dot-type DGS-integrated arc-cornered RMA can be enhanced to 22% with poor polarization purity (10 dB CP–XP isolation) by increasing the width w_d of the defect. The simulated and measured results are presented and the observed phenomena have been justified theoretically to provide a clear insight into the fact.

II. THEORETICAL BACKGROUND AND PARAMETRIC STUDIES

A) Circular dot-type DGS-integrated RMA

Any defect placed beneath the patch alters the fields within the cavity and hence influence the input and radiation characteristics of conventional RMA. The modification of field pattern is based on the geometrical shape of the defect. Therefore, as soon as the dot-type defect is introduced at the close proximity of the non-radiating edges of the patch, the field structure beneath the patch becomes modified. Consequently, the XP radiation decreases in both principal planes and input impedance bandwidth improves.

The defect beneath the patch inevitably introduces some losses in the cavity fields. It increases with the size of dot-type defect and consequently reduces the *Q* factor, which in turn, enhances the impedance bandwidth. The reflection coefficients for different radius r_D of the dot defect are documented in Fig. 2. It is seen that, when r_D increases from 1 to 4 mm, impedance bandwidth increases from 650 MHz (6.5%) to 2.1 GHz (20%). Further increment of r_D is not possible for present structure, as it touches the feeding probe and hence we refrain from investigating the effect of r_D above 4 mm.

Now, the effect of dot defect on the radiation property has been investigated in Figs. 3 and 4. The electric fields of second higher order orthogonal mode (TM_{02}) reside near the non-radiating edges and are significantly responsible for high XP radiation [12, 17]. Moreover, the fields of orthogonal component of dominant mode that lies near the patch corners also

https://doi.org/10.1017/S1759078715001683 Published online by Cambridge University Press

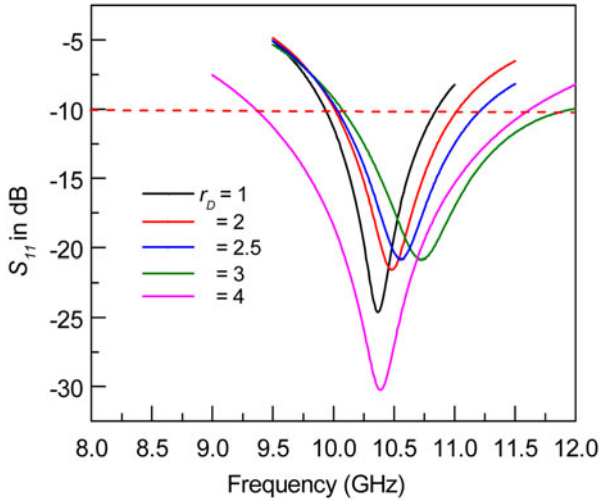

Fig. 2. Reflection coefficient profile as a function of different r_D values for only circular dot-type DGS-integrated RMA (patch length $L = 8$ mm, patch width $W = 14$ mm, substrate thickness $h = 1.575$ mm, and $\varepsilon_r = 2.33$).

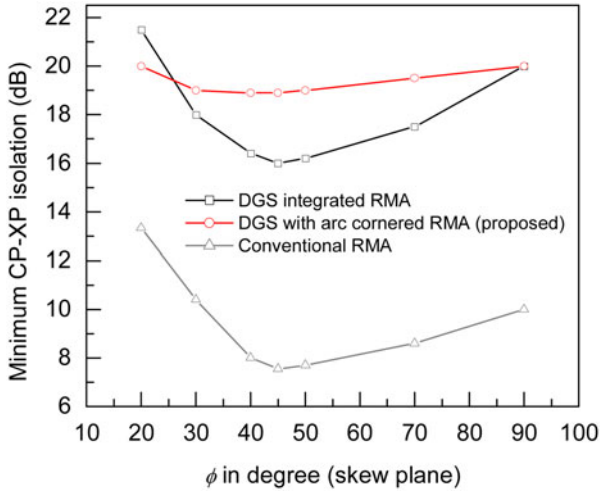

Fig. 4. Variation of minimum CP–XP isolation as a function of skew φ-planes for conventional RMA, only circular dot-type DGS-integrated RMA, and arc-cornered circular dot-type DGS-integrated RMA (parameters as in Fig. 2, for arc-cornered RMA, $r_r = 0.5$ mm, and circular dot radius $r_D = 4$ mm).

contribute to XP radiation as is evident from [11, 14, 15]. Therefore, the present dot defect is judiciously placed in such a way that it can address both the fields for reduction of XP radiation. Figure 3 shows the CP–XP isolation of RMA, as a function of r_D for different skew planes (different φ planes). It is found that as r_D increases, it can perturb more and more electric fields near non-radiating edges and patch corners and hence CP–XP isolation improves. It may be noted that, minimum CP–XP isolation of 20 dB is achieved in principal H-plane ($\varphi = 90^\circ$) for the DGS-integrated RMA, while the same for the conventional RMA is only 10 dB. Similar profile is observed in diagonal $\varphi = 45^\circ$ and 70° planes for different values of r_D as is clear from the figure. However, one very crucial point may be noted from Fig. 3 that, CP–XP isolation for DGS-integrated RMA is different in different skew planes. Figure 4 clearly depicts the fact. It is observed that, CP–XP isolation for DGS-integrated RMA is very good (around 20–22 dB CP–XP isolation) near the E-plane ($\varphi = 0^\circ$), $\varphi = 20^\circ$ planes. But it degrades gradually and become worse (around 16 dB CP–XP isolation) near

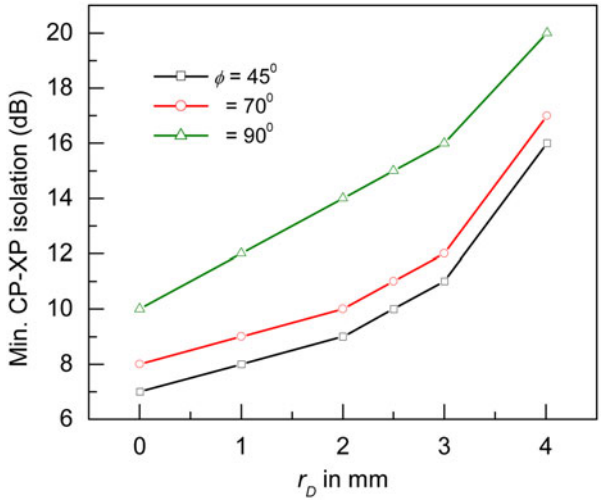

Fig. 3. Variation of minimum CP–XP isolation as a function of r_D for only circular dot-type DGS-integrated RMA at different φ-planes (parameters as in Fig. 2).

diagonal $\varphi = 45^\circ$, 70° planes. However, Fig. 4 depicts that the CP–XP isolation in all planes are much improved for DGS-integrated RMA compared with conventional RMA. Nevertheless, for both the conventional and DGS-integrated RMA, the H-plane CP–XP isolation is far better than diagonal $\varphi = 45^\circ$ plane. It inevitably produces severe limitations to the application where complete polarization purity in all φ-planes is the key issue in a wireless communication link [4, 5].

Based on "Ludwig third definition of XP" and also from [18], the far-field XP can be written as

$$E_{xp} = E_\theta \sin\varphi + E_\varphi \cos\varphi. \tag{1}$$

Following the near-field approach [5], for computation of far-field XP, equivalence theorem along with vector potential approach [19] can be used to obtain the XP field at different φ-planes. The far-field components and radiation integrals as obtained from [19]

$$E_\theta = \frac{-jk e^{-jkr}}{4\pi r} L_\phi, \tag{2}$$

$$E_\phi = \frac{-jk e^{-jkr}}{4\pi r} L_\theta, \tag{3}$$

where k is the propagation vector and L_θ, and L_φ are radiation integrals.

$$L_\theta \propto (M_x \cos\theta\cos\phi + M_y \cos\theta \sin\phi), \tag{4}$$

$$L_\phi \propto (-M_x \sin\phi + M_y \cos\phi), \tag{5}$$

$$M_x = -2E_y, \tag{6}$$

$$M_y = -2E_x, \tag{7}$$

https://doi.org/10.1017/S1759078715001683 Published online by Cambridge University Press

where M_x and M_y are magnetic currents and E_x and E_y are the near-field components. Therefore, using (1)–(3), XP fields at different φ-planes

$$E_{xp} = \frac{-jke^{-jkr}}{4\pi r}\,(L_\phi \sin\phi + L_\theta \cos\phi).$$

Using (4)–(7), we may write

$$E_{xp} \propto 2E_y\,(\cos\theta\cos^2\phi - \sin^2\phi) + 2E_x \sin\phi\cos\phi\,(1+\cos\theta)$$
$$\propto 2E_x\left[\frac{E_y}{E_x}\,(\cos\theta\cos^2\phi - \sin^2\phi) + \sin\phi\cos\phi\,(1+\cos\theta)\right]. \quad (8)$$

Therefore from equation (8), it is found that, at principal E and H-planes ($\varphi = 0^\circ$ and 90°, respectively) XP radiation depends only on the E_y component of near-field, while the same for other skew planes depends on both the E_y and E_x components of near-field. Hence, the shape of the rectangular patch has been modified to modify the near-field components. In fact, the small change in the patch geometry changes the shape of the cavity and hence modifies the near-field distribution. In fact, the sharp edge corners of conventional RMA enhances fringing along corner directions in such a way that the XP radiation increases in diagonal skew planes ($\varphi = 45^\circ$, 70°). Therefore, the corners of the patch need to be modified in order to alleviate the constraint in XP radiation. This gives birth to our proposed structure of arc cornered microstrip antenna. Therefore, in the proposed structure, the E_x component increases and the E_y component decreases in near-field distribution and hence E_y/E_x decreases. This in turn reduces XP fields at all skew planes as is evident from equation (8). The variation of CP–XP isolation at different skew planes for the present proposed patch is depicted in Fig. 4. It shows that, the CP–XP isolation varies only from 18.8 to 20 dB in whole ranges of φ-planes for the proposed DGS-integrated arc-cornered RMA. The similar investigation for conventional and only DGS-integrated RMA shows significant variations in whole ranges of φ-planes. Around 7.5–13.5 and 16–21.5 dB variations are noted from Fig. 4 for conventional and only DGS-integrated RMA, respectively. The near-field distribution for conventional, only DGS-integrated RMA and the proposed DGS-integrated arc-cornered RMA is presented in Fig. 5. It shows that, for conventional RMA, electric fields near radiating and non-radiating edges are similar. On the contrary, when dot DGS is incorporated, electric fields (E_y component) near non-radiating edges decrease. This decrement of electric fields (E_y component) near non-radiating edges is more clear for the proposed DGS-integrated arc-cornered RMA. Figure 5 shows that the fields (E_y component) near non-radiating edges are significantly less than the fields (E_x component) near radiating edges for the proposed arc-cornered microstrip antenna which in fact reduces the E_y/E_x ratio for the proposed antenna. This may be attributed for overall suppression of XP fields in all skew planes.

Now, the variation of input and XP radiation performances as a function of the radius (r_r) of the arcs at the corners of the patch are depicted in Table 1. It is seen that as r_r increases, f_r as well as bandwidth decrease. The slight decrement of f_r toward lower side of the spectrum is due to slight lengthening of the patch length. Therefore, effective W/L as well as h/λ_o are reduced which in turn reduce the bandwidth of the patch [20]. However, no significant changes are observed in XP performance in $\varphi = 90^\circ$ plane. However, at $\varphi = 70^\circ$ and 45° optimum XP improvement is found for $r_r = 0.5$ mm.

B) Rectangular dot-type DGS-integrated RMA

In Section II.A, an arc-cornered RMA on nonlinear circular dot-type defected ground plane has been investigated. With the view of those studies, the similar arc-cornered RMA on linear rectangular-type defected ground plane has been examined in Fig. 6. The dimensions of rectangular defects at four corners of the patch have been chosen with a view to perturb the fields near non-radiating edges, while it keeps the dominant mode field unaltered. At first, a defect with length l_d with thin width $w_d = 1$ mm (so that less perturbation is offered to dominant mode fields beneath the patch) is considered as defect in the ground plane.

Figure 6(a) shows the variation of peak CP gain, CP–XP isolation at $\phi = 90^\circ$ and impedance bandwidth when l_d varies from 3 to 8 mm. The peak CP gain is nearly constant to 4.8–5 dBi in the entire range as is clear from the figure. It may be noted that, when l_d varies from 3 to 6 mm, no significant improvement is observed in XP performance. In fact, when l_d is limited to 6 mm, some portion of non-radiating edges are free to radiate and this may be attributed for appreciable XP radiations. Therefore, CP–XP isolation is not improved much (of the order of 12.5 dB) till $l_d = 6$ mm. Now, beyond $l_d = 6$ mm, CP–XP isolation starts to improve as very small region of non-radiating edges are exposed for XP radiation. Moreover, when $l_d = 8$ mm, the defect occupies full region beneath the non-radiating edges of the patch. This alleviates the radiation from the non-radiating edges completely and improves CP–XP isolation significantly. Around 25 dB of CP–XP isolation at the H-plane is revealed from Fig. 6(a).

If we concentrate on the bandwidth of the antenna, then the gradual improvement of the bandwidth with the increment of l_d is noted from Fig. 6(a). As the defect dimension l_d increases, loss increases which decreases the Q factor and improves the bandwidth of the structure. Around 9% of bandwidth for $l_d = 8$ mm is revealed from Fig. 6(a).

Now, when $l_d = 8$ mm, the effect of width (w_d) of the defect has been examined in Fig. 6(b). It is observed that, when w_d increases from 1 to 8 mm; the peak CP gain decreases gradually. It is also interesting to note from Fig. 6(b) that, as w_d increases, XP performance also degrades. In fact, as the width of the defect increases, back radiation increases. Moreover, the rectangular shape of the defect not only affects the radiating edges, but also perturbs the dominant mode fields at the central region of the patch. These may be attributed for gain reduction of the antenna with w_d. The lowest gain of 2.8 dBi is observed with the rectangular defect of $w_d = 8$ mm as is clear from Fig. 6(b). The unwanted radiation from probe also contributes significantly in XP radiation [21]. Therefore, with the increment of w_d, probe becomes more exposed and enhance XP radiation which in turn degrades CP–XP isolation. It is noted that, the CP–XP isolation and the bandwidth of the antenna with rectangular defects varies in complementary manner with the increment of w_d. Figure 6(b) depicts that when w_d increases from 1 to 4 mm, CP–XP isolation is very good in its H-plane and it is of the order of 22–24 dB. On the contrary, the bandwidth of the antenna is poor for the same values of w_d and it is only of the order of 9–12%. Now, when w_d increases beyond 4 mm,

https://doi.org/10.1017/S1759078715001683 Published online by Cambridge University Press

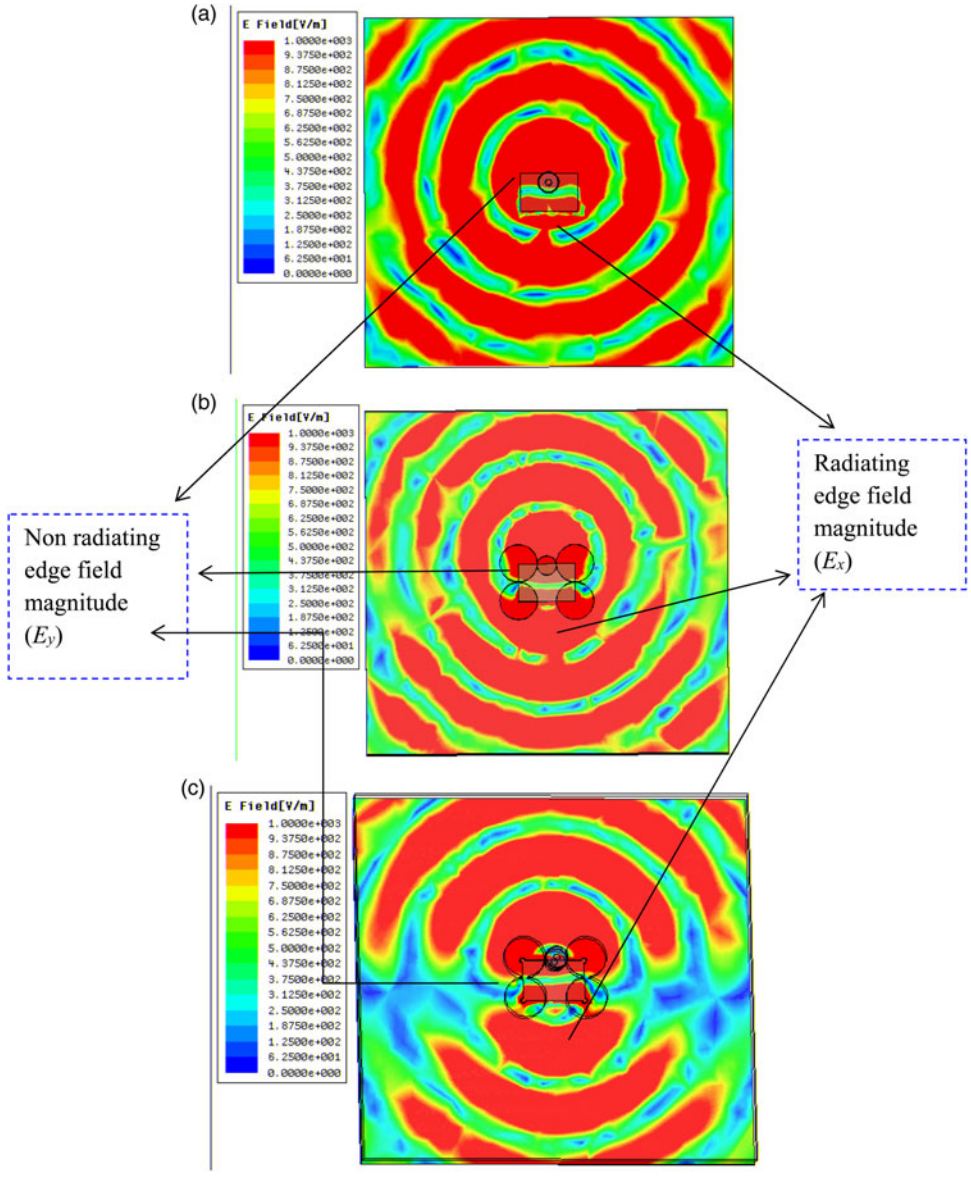

Fig. 5. Near electric field magnitude at radiating and non-radiating edges for: (a) conventional RMA, (b) only circular dot-type DGS-integrated RMA, and (c) arc-cornered circular dot-type DGS-integrated RMA (parameters as in Fig. 2, for arc-cornered RMA, $r_r = 0.5$ mm, and circular dot radius $r_D = 4$ mm).

bandwidth of the antenna increases, while CP–XP isolation decreases. Maximum bandwidth of 22% with poor CP–XP isolation of only 10 dB is noted from Fig. 6(b) when $w_d = 8$ mm.

Table 1. Minimum CP–XP isolation at different φ-planes for proposed arc-cornered circular dot-type DGS-integrated RMA as a function of the radius r_r of the arc at patch corners.

r_r (mm)	% Bandwidth	f_r (GHz)	CP–XP isolation (dB) in $\varphi = 90°$ plane	CP–XP isolation (dB) in $\varphi = 70°$ plane	CP–XP isolation (dB) in $\varphi = 45°$ plane
0.2	20.3	10.32	18.49	17.3	15.82
0.4	20.1	10.1	19.45	17.3	16.14
0.5	20	9.99	20	19	18.85
0.8	16	9.52	20.15	18.5	16.79
1	15.32	9.19	20	17.8	17.94

Therefore, it may be concluded that, the geometrical shape of the defect plays a vital role to modulate the fields beneath the patch for simultaneous improvement in impedance bandwidth and polarization purity of the arc-cornered RMA.

C) Performance of circular dot-type DGS-integrated arc-cornered RMA as a function of ground plane dimension (G)

The performance of the present structure on the square ground plane with dimension $G \times G$ has been investigated in Fig. 7. These reveal some significant variations in gain, bandwidth, and XP performances. It is noted from Fig. 7(a) that, as the ground plane dimension G increases from $0.5\lambda_o$ to $2.5\lambda_o$, the peak gain varies from 2.8 to 5.3 dBi and this variation of gain with the ground plane dimension is periodic in nature as in the case of conventional RMA [22–24]. Consequently, the back radiation varies in opposite manner

https://doi.org/10.1017/S1759078715001683 Published online by Cambridge University Press

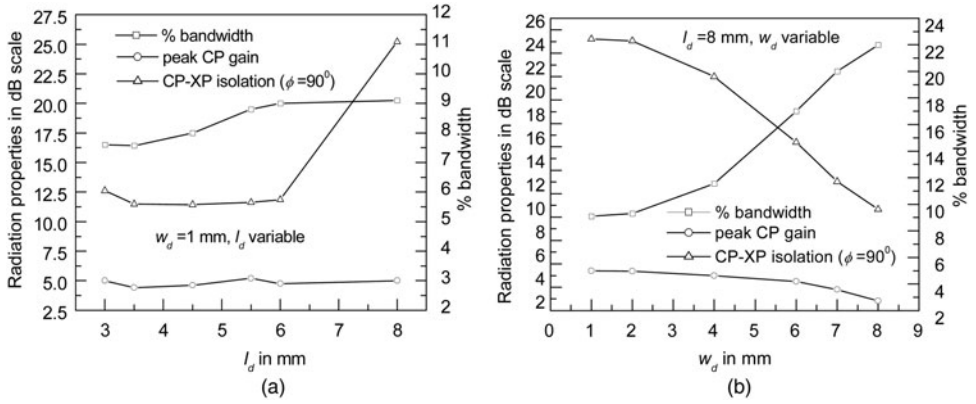

Fig. 6. Impedance bandwidth and radiation properties (peak CP gain and CP–XP isolation) of rectangular dot-type DGS-integrated arc-cornered RMA. (a) w_d = 1 mm, l_d variable and (b) l_d = 8 mm, w_d variable (patch parameters as in Fig. 2, for arc-cornered RMA, r_r = 0.5 mm).

with the ground plane dimension G as it is clear from the figure. Now, if we concentrate on the variation of XP performance as a function of ground plane dimension, some crucial points are observed. Basically, the conventional RMA with an infinite ground plane generate the field patterns that are considerably different in the principal E- and H-planes. The E-plane beam shows that its magnitude does not decrease with the angle excessively from its peak value at broadside. On the contrary, H-plane beam decreases to zero rapidly and hence the H-plane beam width is quite narrower than E-plane beam width. Since the peak XP in the diagonal planes are proportional to the difference of the E- and H-plane patterns, microstrip antennas exhibit large cross-polarizations with an infinite ground plane [23, 24]. So, by reducing the ground plane size, the pattern roll-off increases in the E-plane, but decreases in the H-plane. This in turn brings symmetry in E- and H-plane beams and reduces the gain which in fact decreases the peak XP level in the diagonal planes as is indicated in [23, 24]. But, in the present arc-cornered RMA, the patch geometry is shaped judiciously to modulate the field patterns beneath the patch in a particular manner. This in fact, produces more or less symmetrical radiation beams in both principal planes and accordingly the XP radiation at the diagonal planes are reduced at the cost of the 1–2 dB of decrement in gain for all ground plane dimensions. The maximum gain in the present structure is 5.3 dBi with its XP peak of 13.9 dB at the 45° diagonal planes, while the same for conventional RMA is around 7 dBi with its XP peak of 1 dB at the 45° diagonal planes. However, trivial variation (13.9–15 dB) of the XP peak at the 45° diagonal planes is noted from Fig. 7(a) with the change in ground plane dimension. It reveals that, as G increases from $0.5\lambda_o$ to $2.5\lambda_o$, the XP peak at the 45° diagonal planes increases with the increment in peak gain and decreases with the decrement in peak gain as expected. Nevertheless, the peak XP values at $\phi = 90°$ and 45° matches excellently in all values of G. The resulting CP–XP isolation in both the $\phi = 90°$ and 45° planes as a function of ground plane dimension are depicted in Fig. 7(b). It shows that the CP–XP isolation is similar for both the principal and diagonal planes.

The variation of impedance bandwidth as a function of ground plane dimension is also depicted in Fig. 7(b). The gradual increment of impedance bandwidth with G is apparent from the figure. As the ground plane dimension G increases, it introduces more conduction losses and reduces the Q factor, which may be attributed for this increment in impedance bandwidth with G for the proposed structure.

III. ANTENNA CONFIGURATIONS

An arc-cornered RMA with patch length L = 8 mm, width W = 14.2 mm has been fabricated on PTFE substrate of permittivity ε_r = 2.33, height h = 1.58 mm to operate around the X band. The chosen dimension of the ground plane is 80 × 80 mm^2 ($2.5\lambda_o \times 2.5\lambda_o$) (as suggested from Fig. 7(b) to obtain good bandwidth and polarization performance). At first, four circular

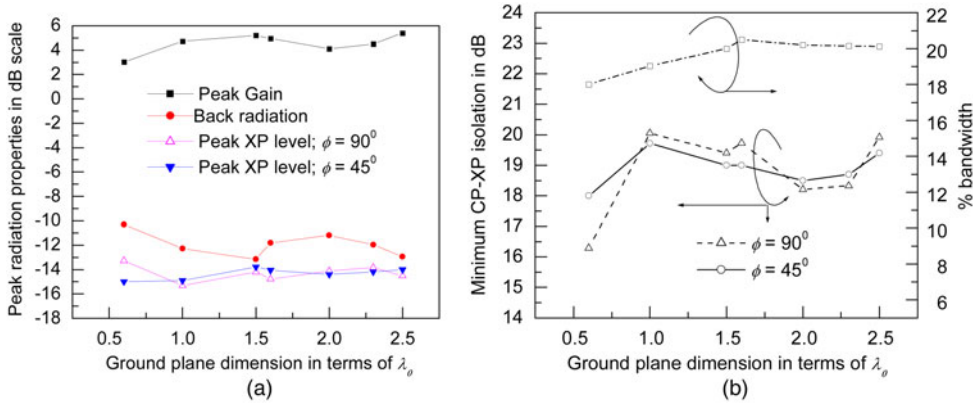

Fig. 7. Performance of circular dot-type DGS-integrated arc-cornered RMA as a function of ground plane dimension (G). (a) Radiation properties and (b) resulting CP–XP isolation and impedance bandwidth (patch parameters as in Fig. 2, for arc-cornered RMA, r_r = 0.5 mm, circular dot radius r_D = 0.5 mm).

https://doi.org/10.1017/S1759078715001683 Published online by Cambridge University Press

dot-type defects of radius $r_D = 4$ mm has been placed at the ground plane and located at four corners of the patch. The four corners of this DGS-integrated rectangular patch have been modified in the shape of circular arc with arc radius $r_r =$ 0.53 mm. This gives birth to our circular dot-type DGS-integrated arc-cornered RMA as shown in Fig. 1. Secondly, four rectangular dot-type defects of dimensions $l_d \times w_d$ (8×8 and 8×1 mm^2, respectively) have been placed at ground plane and located at four corners of the patch. The dimensions of rectangular dot-type defects have been optimized based on the parametric studies documented in Section II.B. The proposed structures are fed at 3.2 mm (circular dot-type DGS) and 2.9 mm (rectangular dot-type DGS) from the center of the patch. The fabricated prototypes are shown in Fig. 8.

IV. RESULTS AND DISCUSSIONS

The simulated [25] and measured results obtained for the conventional and the present structure with circular (Section IV.A) and rectangular dot-type DGS (Section IV.B) are presented. The patch has been excited by a PE4128 SMA connector. Agilent's E8363B network analyzer has been used to obtain the reflection coefficient profiles for the prototypes. The radiation pattern has been measured using Agilent's E4413A CW power sensor (50 MHz –26.5 GHz, −70 to +20 dBm), where Agilent's probe has been used to pick up the received signal. Agilent's E4418B single channel power meter is utilized for the measurement.

A) Circular dot-type DGS-integrated arc-cornered RMA

Figure 9 shows the simulated and measured reflection coefficient profile for both the conventional and present (circular dot-type DGS-integrated arc-cornered RMA) structures.

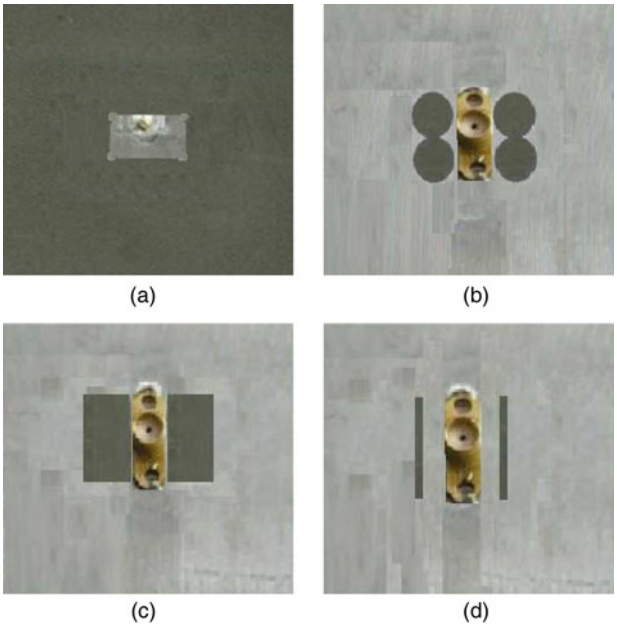

Fig. 8. Photograph of fabricated arc-cornered DGS-integrated RMA. (a) Top view, (b) bottom view for the circular dot-type DGS ($r_D = 4$ mm), (c) bottom view for the rectangular dot-type DGS ($l_d \times w_d = 8 \times 8$ mm^2), and (d) bottom view for the rectangular dot-type DGS ($l_d \times w_d = 8 \times 1$ mm^2).

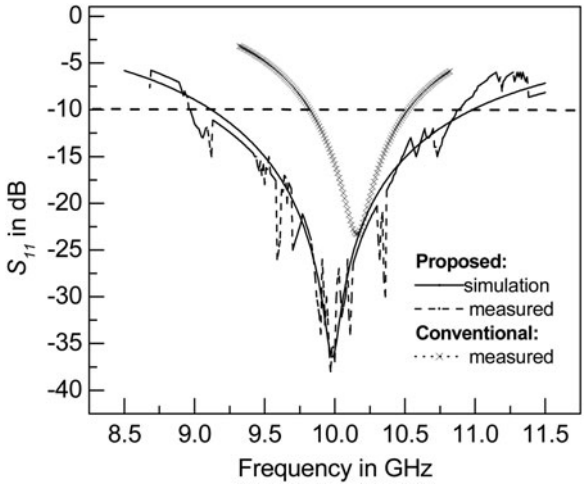

Fig. 9. Reflection coefficient profile for the conventional RMA and the proposed arc-cornered DGS-integrated RMA.

Both the antennas are resonant near 10 GHz and the obvious indication of band width enhancement with the proposed structure is revealed from the figure. Around 20% band width is achieved with the present arc-cornered DGS-integrated RMA, while the same for the conventional RMA is only around 6.5%. Close mutual agreement between the simulation and measured results is apparent from Fig. 9.

Figure 10(a) shows the *H*-plane radiation pattern for both the conventional and present (circular dot-type DGS-integrated arc-cornered RMA) structures at $f = 10.1$ GHz. Around 20 dB of CP–XP isolation is evident from the proposed structure, while the same for the conventional is around 9.5 dB for the wide angular region near the broadside direction. Similar improvement of CP–XP isolation is apparent in the *H*-plane for the other two frequencies in the operating band (Figs 10(b) and 10(c) for $f = 9.61$ and 10.8 GHz, respectively). As the XP fields in the *E*-plane is insignificant, we refrain from giving the results in the *E*-plane.

Figure 11 represents the XP performance of the present arc-cornered circular dot-type DGS-integrated RMA at different diagonal skew planes at different frequencies over the operating band. The developed in house facilities have been utilized for measurements of radiation patterns at different skew planes. Figure 11(a) represents the measured radiation performance of the present antenna at $\varphi = 30^\circ$, 45°, and 75° for center frequency $f = 10$ GHz. Around 19, 19.3, and 20 dB of the CP–XP isolation is revealed at $\varphi = 30^\circ$, 45°, and 75°, respectively. Similar investigation with the conventional RMA and only DGS-integrated RMA shows that the XP performance is different in different skew planes (not shown in the paper). On the contrary, the present arc-cornered DGS-integrated RMA show the nearly identical CP–XP isolation over all skew planes. Figs 11(b) and 11(c) show the similar investigation at $f = 9.61$ and 10.8 GHz, respectively. Both the figures depict that the CP–XP isolation is same in all over the skew planes. However, the CP radiation profile is not shown in Fig. 11(c) as it is similar for all the cases. Hence, the present structure maintains its uniformity in CP–XP isolation over different diagonal skew planes in the whole operating band. However, it may be noted that the CP–XP isolation are slightly increasing (around 1.7 dB) with the frequency. In fact, this is due to the increment of XP level with increase in frequency [2, 3]. Therefore, it may be concluded that the complete

https://doi.org/10.1017/S1759078715001683 Published online by Cambridge University Press

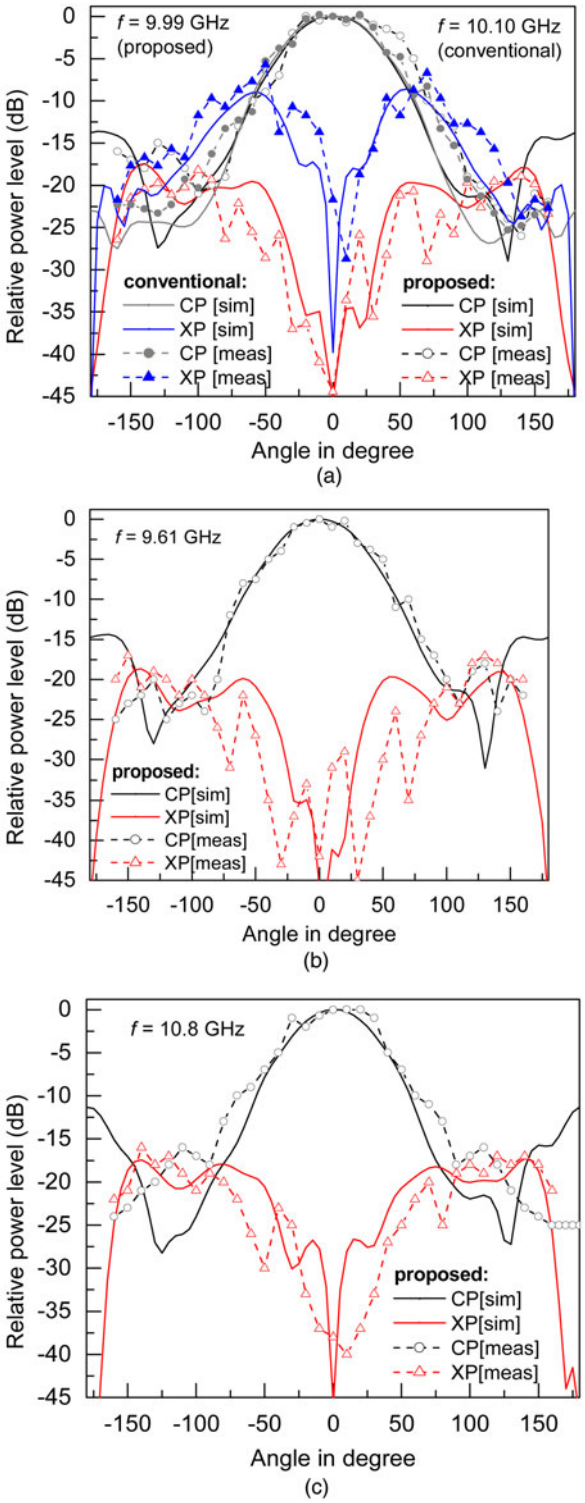

Fig. 10. Simulated and measured *H*-plane radiation patterns at different frequencies. (a) Comparison between circular dot-type DGS-integrated arc-cornered RMA and conventional RMA at $f = 9.99$ GHz (present RMA), 10.1 GHz (conventional RMA), (b) present RMA at $f = 9.61$ GHz, and (c) present RMA at $f = 10.8$ GHz.

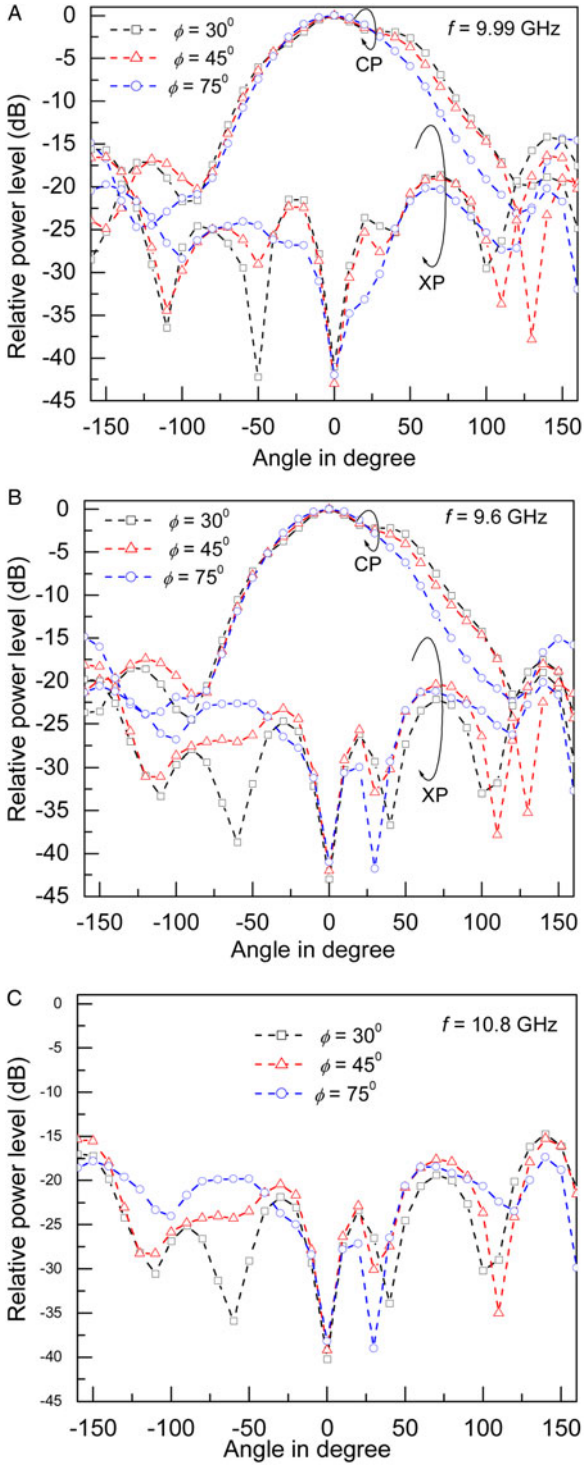

Fig. 11. Measured radiation patterns at different skew planes at different frequencies for the present circular dot-type DGS-integrated arc-cornered RMA. (a) $f = 9.99$ GHz, (b) $f = 9.61$ GHz, and (c) $f = 10.8$ GHz.

XP suppression can be achieved with the present structure, which is not possible with the conventional RMA and only DGS-integrated RMA. Hence, the new antenna is very much helpful for the scientific community looking for good CP–XP isolation completely in all planes.

B) Rectangular dot-type DGS-integrated arc-cornered RMA

The measured results obtained for the present arc-cornered RMA with rectangular dot-type DGS are presented in Figs. 12 and 13. The observations from the measured results show the close resemblance of input and radiation properties of the structure with the simulation studies depicted in Section

https://doi.org/10.1017/S1759078715001683 Published online by Cambridge University Press

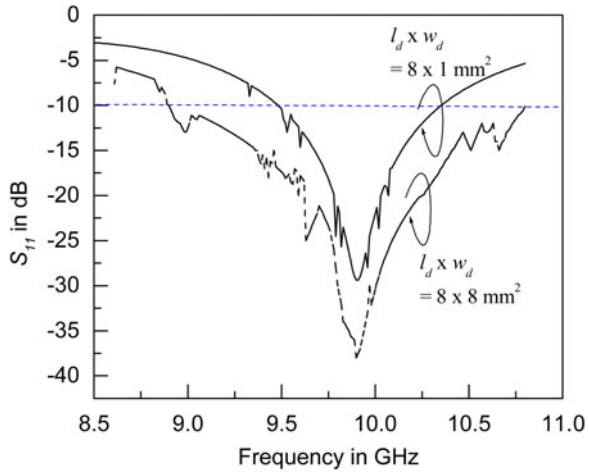

Fig. 12. Measured reflection coefficient profiles for rectangular dot-type DGS-integrated arc-cornered RMA with $l_d = 8$ mm, $w_d = 1$ and 8 mm.

II.B. The optimum defect dimensions $l_d \times w_d$ for the prototypes are chosen as 8×8 and 8×1 mm^2 for better bandwidth and cross-polarization performances respectively as suggested in Section II.B.

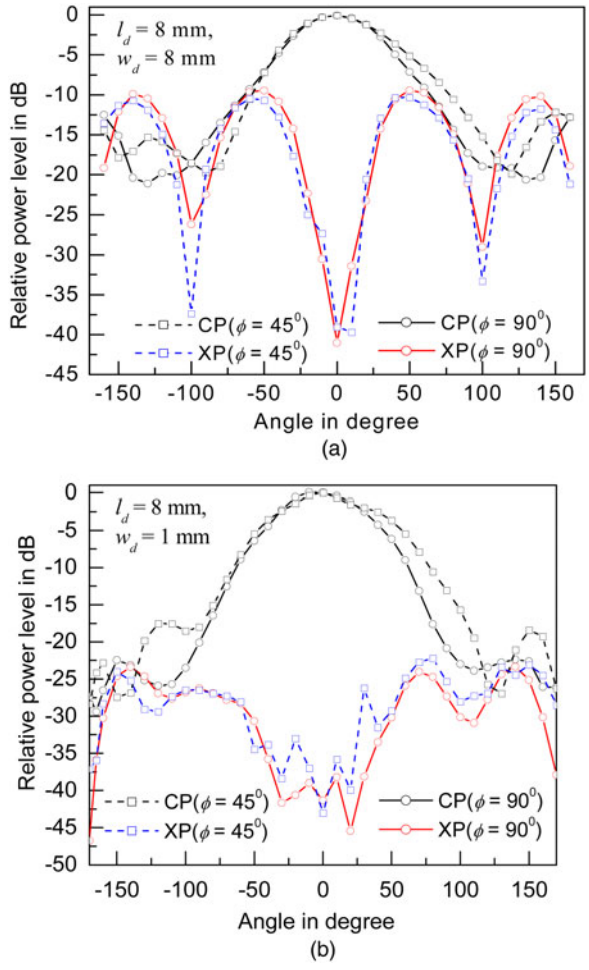

Fig. 13. Measured radiation patterns for rectangular dot-type DGS-integrated arc-cornered RMA in the principal H- and 45° diagonal planes at center frequency $f = 9.98$ GHz. (a) $l_d = 8$ mm, $w_d = 8$ mm and (b) $l_d = 8$ mm, $w_d = 1$ mm.

Figure 12 shows the reflection coefficient profiles for both the prototypes. A significant disparity in the bandwidth performance for two structures is noted. It is evident from Fig. 12 that the measured impedance bandwidth of the structure with $l_d = 8$ mm and $w_d = 8$ mm is around 21.3%, while the same with $l_d = 8$ mm and $w_d = 1$ mm is only 8.7%. In fact, the increment of loss due to larger dimensions of the defect lowers the cavity Q factor, and increases the bandwidth of the structure as discussed in Section II.

The radiation properties for both the prototypes are depicted in Fig. 13 for $l_d \times w_d = 8 \times 8$ and 8×1 mm^2, respectively. The measured gain of the structure with $w_d = 8$ mm is 2.6 dBi, while the same for $w_d = 1$ mm is 4.7 dBi. Consequently, significant back radiations in terms of CP and XP are noted from Fig. 13(a) for the case with $w_d = 8$ mm. The CP–XP isolation for the structure is poor and it is of the order of 11 dB only. On the contrary, less back radiation along with excellent CP–XP isolation of around 24.5 dB is revealed from Fig. 13(b) for $w_d = 1$ mm. However, it is interesting to note that the CP–XP isolation in the principal H-plane and diagonal 45° plane is similar for both the cases with $w_d = 8$ and 1 mm.

Therefore, for rectangular dot-type DGS-integrated arc-cornered RMA; the defect dimensions should be chosen properly based on the requirements of bandwidth and polarization performances.

V. CONCLUSION

A new arc-cornered microstrip antenna integrated with a circular and rectangular DGS have been investigated for significant improvement in bandwidth and CP–XP isolation of microstrip patch in all planes The present structures can provide wide impedance bandwidth (20%) along with 20–25 dB CP–XP isolation in principal and diagonal skew planes. The proposed geometry is very simple, easy to fabricate, and therefore help in the effortlessness manufacturing process. The new antenna is definitely be useful for wireless communication systems where uniform polarization purity is required in principal and all diagonal skew planes.

ACKNOWLEDGEMENTS

The authors would like to thank Professor D. Guha of Institute of Radio Physics and Electronics and A. Ghosh of Department of ECE, Mizoram University for their support by which the whole theoretical fact is established in the present form.

REFERENCES

[1] Kumar, G.; Ray, K.P.: Broadband Microstrip Antennas, Artech House, Norwood, MA, USA, 2003.

[2] Guha, D.; Antar, Y.M.M. (eds): Microstrip and Printed Antennas – New Trends, Techniques and Applications, Wiley, UK, 2011.

[3] Garg, R.; Bhartia, P.; Bahl, I.; Ittipiboon, A.: Microstrip Antenna Design Handbook, Artech House, Norwood, USA, 2001.

[4] Hansen, R.: Cross polarization of microstrip patch antennas. IEEE Trans. Antennas Propag., **35** (1987), 731–732.

https://doi.org/10.1017/S1759078715001683 Published online by Cambridge University Press

[5] Bhardwaj, S.; Samii, Y.R.: Revisting the generation of cross polarization in rectangular patch antennas: a near field approach. IEEE Antennas Propag. Mag., **56** (2014), 14–38.

[6] Chen, Z.N.; Chia, M.Y.W.: Broad-band suspended probe-fed plate antenna with low cross-polarization levels. IEEE Trans. Antennas Propag., **51** (2003), 345–346.

[7] Islam, M.T.; Shakib, M.N.; Misran, N.: Design analysis of high gain wideband L-probe fed microstrip patch antenna. Prog. Electromagn. Res., **95** (2009), 397–407.

[8] Yang, F.; Zhang, X.; Ye, X.; Samii, Y.R.: Wide-band E-shaped patch antennas for wireless communications. IEEE Trans. Antennas Propag., **49** (2001), 1094–1100.

[9] Sharma, S.K.; Shafai, L.: Performance of a novel Ψ -shape microstrip patch antenna with wide bandwidth. IEEE Antennas Wireless Propag. Lett., **8** (2009), 468–471.

[10] Heydari, R.D.; Moghadasi, M.N.: Introduction of a novel technique for the reduction of cross-polarization of rectangular microstrip patch antenna with elliptical DGS. J. Electromagn. Wave Appl., **22** (2008), 1214–1222.

[11] Kumar, C.; Guha, D.: DGS integrated rectangular microstrip patch for improved polarization purity with wide impedance bandwidth. IET Microw. Antennas Propag., **8** (2014), 589–596.

[12] Ghosh, A.; Ghosh, D.; Chattopadhyay, S.; Singh, L.L.K.: Rectangular microstrip antenna on slot type defected ground for reduced cross polarized radiation. IEEE Antennas Wireless Propag. Lett., **14** (2015), 321–324.

[13] Ghosh, A.; Ghosh, S.K.; Ghosh, D.; Chattopadhyay, S.: Improved polarization purity for circular microstrip antenna with defected patch surface. Int. J. Microw. Wireless Technol., (2014). DOI: 10.1017/S1759078714001305.

[14] Chakraborty, S.; Ghosh, A.; Chattopadhyay, S.; Singh, L.L.K.: Improved cross polarized radiation and wide impedance bandwidth from rectangular microstrip antenna with dumbbell shaped defected patch surface. IEEE Antennas Wireless Propag. Lett., (2015). DOI: 10.1109/LAWP.2015.2430881.

[15] Ghosh, A.; Chakraborty, S.; Chattopadhyay, S.; Nandi, A.; Basu, B.: Rectangular microstrip antenna with dumbbell shaped defected ground structure for improved cross polarized radiation in wide elevation angle and its theoretical analysis. IET Microw. Antennas Propag., DOI: 10.1049/iet-map.2015.0179.

[16] Chakraborty, S.; Chattopadhyay, S.: Substrate fields modulation with defected ground structure: a key to realize high gain, wideband microstrip antenna with improved polarization purity in principal and diagonal planes. Int. J. RF, Microw. Comput. Aided Eng., DOI: 10.1002/mmce.20950.

[17] Ghosh, D. et al.: Physical and quantitative analysis of compact rectangular microstrip antenna with shorted non-radiating edges for reduced cross-polarized radiation using modified cavity model. IEEE Antennas Propag. Mag., **56** (2014), 61–72.

[18] Lee, K.F.; Luk, K.M.; Tam, P.Y.: Cross polarization characteristics of circular patch antennas. Electron. Lett., **28** (1992), 587–589.

[19] Balanis, C.A.: Antenna Theory and Design, 3rd ed., Wiley, New York, 2004.

[20] Jackson, D.R.; Alexopoulos, N.G.: Simple approximate formulas for input resistance, bandwidth, and efficiency of a resonant rectangular patch. IEEE Trans. Antennas Propag., **39** (1991), 407–410.

[21] Kumar, C.; Guha, D.: Nature of cross-polarized radiation from probe fed circular microstrip antenna and their suppression using different geometries of DGS. IEEE Trans. Antennas Propag., **60** (2012), 92–101.

[22] Chattopadhyay, S.; Siddiqui, J.Y.; Guha, D.: Rectangular microstrip patch on a composite dielectric substrate for high gain wide beam radiation patterns. IEEE Trans. Antennas Propag., **57** (2009), 3324–3327.

[23] Noghaanian, S.; Safai, L.: Control of microstrip antenna radiation characteristics by ground plane size and shape. IEE Proc. Microw. Antennas Propag., **145** (1998), 207–212.

[24] Kishk, A.A.; Safai, L.: The effect of various parameters of circular microstrip antenna on their radiation efficiency and the mode excitation. IEEE Trans. Antennas Propag., **34** (1986), 969–976.

[25] HFSS: High Frequency Structure Simulator, Version 14, Ansoft Corp, USA.

Subhradeep Chakraborty was born in Siliguri, West Bengal, India on October 20, 1990. He received his B. Tech. and M. Tech. degrees from West Bengal University of Technology in 2012 and 2014, respectively. During M. Tech, he worked with CSIR-CEERI, Pilani, India. Presently, he is attached with Siliguri Institute of Technology as a research scholar. He is pursuing his research under the supervision of Dr. Sudipta Chattopadhyay. He has some significant contributions in the field of microstrip antennas. His area of research includes defected ground structure in microstrip antennas, planar antennas, fast wave, and high-power microwave tubes.

Sudipta Chattopadhyay was born in Kolkata, India on September 10, 1974. He received his B.Sc. (Physics Honors) degree from the University of Calcutta in 1996 and B. Tech., M. Tech., and Ph.D. degrees from the Institute of Radio Physics and Electronics, the University of Calcutta in 1999, 2001, and 2011, respectively. He is currently working as an Associate Professor of Siliguri Institute of Technology, West Bengal, India. He is listed in Marquis Who's Who in the World, USA, 26th Ed, 2009 and also listed in 2000 Outstanding Intellectuals of the 21st Century, UK, 2010. He serves as the reviewer of IEEE Antennas and Propagation Magazine; IEEE Antennas and Wireless Propagation Letters; IET Microwave Antennas and Propagation Journal, UK; and Journal of Microwaves, Optoelectronics and Electromagnetic Applications, Brazil. He has more than 50 publications in referred international journals and international conferences. His area of research includes microwave antennas, microstrip, and integrated antennasand computer-aided design of patch antennas.